Korean J. Chem. Eng., 37(3), 513-524 (2020)
DOI: 10.1007/s11814-019-0433-5

pISSN: 0256-1115
eISSN: 1975-7220

CO_2 and N_2 adsorption and separation using aminated UiO-66 and $Cu_3(BTC)_2$: A comparative study

Kasra Pirzadeh, Kourosh Esfandiari, Ali Asghar Ghoreyshi†, and Mostafa Rahimnejad

Chemical Engineering Department, Babol Noshirvani University of Technology, Babol, Iran
(*Received 7 September 2019 • accepted 17 November 2019*)

Abstract−UiO-66 and $Cu_3(BTC)_2$, two well-known metal organic frameworks (MOFs), were aminated through in-situ modification approach to improve CO_2/N_2 separation. UiO-66 was synthesized by solvothermal method, while $Cu_3(BTC)_2$ was synthesized with two electrochemical and solvothermal approaches for the sake of comparison. NH_2-UiO-66 structure was optimized by evaluating the effect of key parameters, such as synthesis temperature, ligand to metal salt molar ratio, and modulator to metal salt molar ratio, on CO_2/N_2 selectivity. The effect of different weight percentage of 2-aminoterephthalic acid (NH_2-BDC) on electrochemical synthesis of NH_2-$Cu_3(BTC)_2$ was also investigated. Products were characterized by FTIR, BET, FESEM, XRD, and TGA analyses. Single CO_2 adsorption experiment for NH_2-UiO-66 showed higher capacity compared to UiO-66. However, for NH_2-$Cu_3(BTC)_2$, an opposite trend was observed. The CO_2 adsorption capacity for NH_2-UiO-66 and NH_2-$Cu_3(BTC)_2$ at 1 bar and 25 °C was 3.32 and 3.86 mmol/g, respectively. CO_2/N_2 selectivity with fixed concentration ratio (15/85 vol%) was also studied for aminated samples, and the values of 120 and 53 were determined for NH_2-UiO-66 and NH_2-$Cu_3(BTC)_2$, respectively. NH_2-$Cu_3(BTC)_2$ showed the highest isosteric heat of adsorption among all samples (43 kJ/mol).

Keywords: NH_2-UiO-66, NH_2-$Cu_3(BTC)_2$, CO_2/N_2 Adsorption, Selectivity

INTRODUCTION

Currently, about 86% of energy demand in industrial plants is provided by fossil fuels, which results in massive CO_2 emission to the atmosphere. Hence, finding ways to control the CO_2 emission to mitigate global warming is crucial. Among different methods for CO_2 capture and sequestration, absorption-based processes using aqueous alkanolamines have been applied for decades. However, these methods suffer from several drawbacks, such as high energy consumption and low CO_2 loading capacity [1,2]. Carbon Capture and Storage (CCS) in porous materials is another technique with many advantages compared to other technologies, mainly less energy consumption, higher selectivity, and minimal environmental impacts [3]. Carbon based materials such as metal oxides [4], zeolites [5,6], and organic-inorganic frameworks [7,8] are well-stablished materials for CCS processes.

Covalent organic framework (COF) and metal organic framework (MOF) are two subclasses of organic-inorganic framework. These porous coordination polymers, due to their tunable porosity, flexible structure, and high surface area [9,10], have been chosen as viable candidates for various applications such as gas storage [11,12], drug delivery [13,14], catalysis [15,16], and sensors [17]. COFs are emerging class of porous crystalline polymers comprised of light elements such as H, C, N, B and O, which crystallize into 2D layers or 3D networks [18]. Among various COFs, covalent triazine frameworks (CTFs) have been widely used in CO_2 adsorption due to its nitrogen-rich nature. Its high nitrogen content and considerable surface area can improve CO_2 capture through physisorption π system. CTFs are also capable to be functionalized by polar functional groups such as inorganic ions or oxygen containing groups [19]. Furthermore, COFs can also be applied in thin films in which they act as 2D templates by introducing adsorbed molecules into the system. By means of this strategy functional surfaces that would be beneficial for CO_2 adsorption could be formed; however, this potential application needs to be more developed [20]. On the other hand, MOFs have been developed as a class of crystalline materials that consist of infinite inorganic nodes interconnected by organic linkers [21,22]. Among numerous identified and synthesized MOFs, many of them have been used in CCS process based on their characteristics, such as $Cu_3(BTC)_2$, MIL-101, CPM-5, MOF-177, UiO-66 [23]. The present study deals with synthesize and application of two well-known MOFs (i.e., $Cu_3(BTC)_2$ and UiO-66) in CO_2/N_2 separation. UiO-66 is one of the Zr-based MOFs which is constructed of six Zr cations coordinated by square-antiprismatic geometry connected to eight oxygen atoms forming a secondary building unit (SBU). Each SBU is interconnected to twelve ditopic 1,4-benzenedicarboxylate (BDC) that form octahedron and tetrahedron cages with pore sizes of 11 and 8 Å, respectively [24]. UiO-66 has attracted much interest due to its high thermal stability (up to 500 °C), its high resistance to humidity [25,26], and keeping its crystalline structure after treatment in acidic (pH=1) and basic (pH=14) medium [27]. On the other hand, $Cu_3(BTC)_2$ is another well-known MOF with similar geometry to UiO-66 (octahedral). However, the main pore diameter, corner tetrahedral pockets, and connecting triangular channels are different in size. The SBU of $Cu_3(BTC)_2$ includes paddle-wheel type metal corners bounded

†To whom correspondence should be addressed.
E-mail: aa_ghoreyshi@nit.ac.ir
Copyright by The Korean Institute of Chemical Engineers.

to four tricarboxylate linkers. The crystalline structure of $Cu_3(BTC)_2$ has large central cavities (pore size of 9 Å) surrounded by small pockets (pore size of 5 Å). These side channels are connected through triangular windows of 3.5 Å which forms the central cage of crystal structure [28]. This kind of MOF has shown good affinity to CO_2 molecules due to unsaturated metal sites that would be available after the activation step.

For gas adsorption and separation, amine functionalization is a frequent technique to boost the adsorption capacity and CO_2/N_2 selectivity. It is possible to modify the surface of BDC linker available in the synthesis solution of UiO-66 by introducing -NH_2 functional groups to form NH_2-UiO-66 MOF. In other words, NH_2-UiO-66 is constructed of zirconium metal clusters and 2-amino-1,4-benzene dicarboxylate (NH_2-BDC) ligand with the same topology of UiO-66, which turns it to an interesting material for CO_2 adsorption [29]. In the case of $Cu_3(BTC)_2$ amination, since synthesis of amine functionalized BTC linkers is comprised of a series of complex reactions, a mixture of ligands, i.e., BTC and NH_2-BDC, were employed with different mixing ratios to form NH_2-$Cu_3(BTC)_2$ [30].

Note that using NH_2-BDC ligand in synthesis of amino modified MOFs may bring different results. In NH_2-$Cu_3(BTC)_2$, the presence of aminated ligand may cause some distortion in octahedral structure of $Cu_3(BTC)_2$, since this linker occupies the place of one carboxylate group (out of three) of BTC linker, which would cause a reduction in coordination number of copper atoms. Consequently, a gap would be generated between copper dimmer and linker molecule. However, NH_2-BDC keeps the crystalline structure of MOF intact and neither sign of distortion nor defect could be observed in NH_2-UiO-66 structure.

In this research, two synthesis approaches (solvothermal and electrochemical) were applied for $Cu_3(BTC)_2$ synthesis and the results were compared. Then, the one with better textural properties and higher CO_2 adsorption capacity was selected for further actions. Regarding the synthesis of UiO-66, since Zr electrode could not be provided, conventional solvothermal method was chosen as the synthesis procedure. Afterward, amine functionalization of these two MOFs was performed to study the effect of amination on separation of CO_2 from N_2. For this purpose, ideal adsorbed solution theory (IAST) was applied to determine CO_2/N_2 selectivity by means of data obtained from single gas adsorption experiments. Note that the reason for choosing UiO-66 and $Cu_3(BTC)_2$ for this study was, first, related to similar crystal structures (i.e., octahedral shape) and the presence of open metal sites in the structure of these MOFs that can interact with CO_2 molecules. Second, UiO-66 is of particular interest due to its ease of exchanging functional groups on the terephthalic linker that can cause a change in the adsorption properties of this MOF [25]. However, because of limitation in using aminated form of H_3BTC, a mixture of ligands (as mentioned earlier) was applied for NH_2-$Cu_3(BTC)_2$ synthesis. Therefore, the comparison of CO_2 adsorption capacities, between an MOF with aminated ligand and the one with mixture of ligands, was another reason for picking up these two types of MOFs.

The present study shows some novelties compared to the abundant literature available on amino-modified MOFs for some reasons. First, two synthesis methods (solvothermal and electrochemical) of $Cu_3(BTC)_2$ were compared to determine which one could result in better physical characteristics as well as CO_2 adsorption. Moreover, from synthesis point of view, the electrochemical synthesis method was more convenient, easier to control and implemented in shorter time compared to solvothermal one. Second, the electrochemical technique was applied successfully for the first time to synthesize NH_2-$Cu_3(BTC)_2$. Third, CO_2/N_2 selectivity of 120, which was obtained by NH_2-UiO-66, was among the highest values that has been reported for this type of MOF so far. Fourth, unlike the default premises, it was revealed that amine functionalization does not necessarily improve CO_2 adsorption on MOFs; however, it could improve CO_2/N_2 selectivity due to changes happening in textural properties as well as surface chemistry of the adsorbent.

MATERIALS AND METHODS

1. Materials

All chemical substances including, terephthalic acid (H_2BDC), 2-amino terephthalic acid (NH_2-BDC), $ZrCl_4$, 1,3,5-benzen tricarboxylic acid (H_3BTC), ethanol, tetrabutyl ammonium tetrafluoro borate (TBATFB), dimethyl formamide (DMF) and acetic acid (CH_3COOH) were purchased from Sigma-Aldrich and Merck without further purification. CO_2 (99.99%) and N_2 (99.99%) pure gases were purchased from Faran Gas Co., Iran.

2. Synthesis Procedure

2-1. Synthesis and Amination of UiO-66

UiO-66 was synthesized based on previous report [31] with small modifications in crystals purification step in which, instead of soaking precipitates in methanol for three days, they were stirred in ethanol vigorously for three times and each time for one hour. Typically, 0.223 g $ZrCl_4$ was dissolved in 50 ml DMF and then sonicated for 10 min. Afterward, 0.174 g BDC was added and the solution was sonicated for another 10 min. Then, 2 ml acetic acid as a modulator was introduced to the resulting solution and the solution sonicated for 5 min prior to be transferred into the Teflon-lined autoclave. The autoclave was placed in an oven for 24 h at 120 °C. The system was cooled to room temperature for 8 h. The precipitates were collected by means of centrifuge and washed with DMF for three times and subsequently the solvent was exchanged by ethanol to remove residual DMF from interior parts of the product. Finally, the product was dried for 12 h at 120 °C. NH_2-UiO-66 was also synthesized similar to the UiO-66 procedure except that NH_2-BDC was used as ligand.

Influential parameters considered for optimization of NH_2-UiO-66 synthesis procedure were ligand-to-metal salt molar ratio (S : L), modulator-to-metal salt molar ratio (S : M), and synthesis temperature. In this study, optimization was based on the one factor at a time method (OFAT) to find the adsorbent with the highest CO_2/N_2 selectivity. Range of values associated with each parameter was 1.0-1.5, 0.5-1.0, and 100-140 °C for S : L, S : M, and synthesis temperature, respectively.

2-2. Synthesis and Amination of $Cu_3(BTC)_2$

Solvothermal synthesis procedure of $Cu_3(BTC)_2$ was adapted from our previous report [32] in which 1.75 g copper (II) nitrate trihydrate and 0.84 g H_3BTC were mixed in 48 ml pure ethanol for 30 min. Then, the homogeneous solution was transferred into a Teflon-

lined autoclave and placed in an oven for 14 h at 120 °C. After the reaction was completed, the autoclave was cooled. The precipitates were collected, washed with ethanol and centrifuged for three sequential cycles. Finally, the crystals were dried at 100 °C overnight.

$Cu_3(BTC)_2$ synthesis via electrochemical route was implemented based on our previous study with some modifications [33]. Two copper electrodes with 6 cm^2 effective area spaced 1 cm from each other, placed in the electrolysis cell filled with 100 ml ethanol. 1 g H_3BTC and 0.65 g TBATFB were used as ligand and electrolyte salt, respectively. A constant voltage (25 V) was applied between two electrodes for 2 h. Gradually, a thin layer of MOF formed on the surface of the anode and precipitated at the bottom of the cell. When the synthesis process finished, precipitates were collected and centrifuged twice. In each run, the used solvent was replaced with a fresh one to remove unreacted ligands. Finally, the solid phase was dried and activated in oven for 12 h at 150 °C.

For the synthesis of NH_2-$Cu_3(BTC)_2$, since aminated form of the trimesic acid linker (H_3BTC) was not possible to synthesize [30], a mixture of H_3BTC and NH_2-BDC was applied. In this regard, different weight percentages of NH_2-BDC (10, 20 and 25 wt%) were combined with H_3BTC to study the performance of final product around CO_2 separation from N_2.

3. Characterization Techniques

Adsorption-desorption isotherms of nitrogen were measured by BELSORP mini II at 77 K under pressure ranges 0-100 kPa, after the samples were pretreated at 150 °C for 3 h. The BET surface area, micropore volume, and micropore size distribution were calculated by Brunauer-Emmett-Teller (BET), t-plot, and micropore (MP) plot, respectively. The presence of amine group in NH_2-UiO-66 and NH_2-$Cu_3(BTC)_2$ was investigated by Fourier transform infrared (FTIR) spectroscopy (Spectrometer Spectrum 65 - PERKIN-ELMER, USA). Each scan was obtained by applying definite number of scans in the range of 400-4,000 cm^{-1} with the resolution of 4 cm^{-1}. Thermogravimetric analysis (TGA) was carried out for determining thermal stability of samples (Rheometric Scientific, STA 1500, USA) under air flow at the heating rate of 10 °C/min from room temperature to 800 °C. X-ray diffraction (XRD) patterns were employed to determine the probable variation in crystalline structure of samples after amine modification using X-Pert Pro diffractometer (Germany). This analysis was implemented in 2θ=5-80 ° with accelerator voltage of 40 kV and current of 40 mA. Finally, the morphology of MOFs was characterized by field emission scanning electron microscopy (FESEM) analysis (FEI NOVA NANOSEM 450, USA) at 15 kV for better conductivity.

4. Gas Adsorption Measurements

CO_2 and N_2 adsorption on as-synthesized MOFs were studied experimentally through volumetric method, which was described in detail in our previous report [33]. All experiments were performed over a pressure range of 0-7 bar and at different adsorption temperatures (25, 35, and 45 °C). CO_2/N_2 selectivity was calculated based on ideal adsorption solution theory (IAST) which is well described in supporting information (section 1).

RESULTS AND DISCUSSION

1. Optimization of NH_2-UiO-66 Synthesis Procedure

1-1. Effect of Synthesis Temperature

Temperature is one of the crucial items that must be considered in synthesis of MOFs. For this purpose, three different temperatures (100, 120 and 140 °C), were considered for NH_2-UiO-66 synthesis (samples are called NHU-100, NHU-120 and NHU-140, respectively) and the synthesis procedure was implemented at a fixed S : L : M molar ratio (1.0 : 1.25 : 0.75). Table 1 (Part I) summarizes the obtained results from BET analysis for samples synthesized at aforementioned temperatures. From Table 1 it is clear that the textural properties of NHU-100 and NHU-140 samples are lower than NHU-120, which would undoubtedly influence the gas adsorption capacity. Although increasing the synthesis temperature (up to 120 °C) improves the crystallinity of NH_2-UiO-66, further increase in the synthesis temperature may cause slight agglomeration due to rapid crystal growth, which in turn results in lower CO_2/N_2 selectivity [34]. This result can also be inferred from FESEM images (Fig. 1) in which clear octahedral structures can be observed for NHU-120 (Fig. 1(b)). However, in the case of Fig. 1(a) which belongs to

Table 1. Effect of synthesis parameters on textural characteristics of NH_2-UiO-66 and comparison of optimum sample with textural properties of UiO-66

	Code	Temp. (°C)	S : L molar ratio	S : M molar ratio	S_{BET} (m^2/g)	Pore volume (cm^3/g)	Average pore diameter (nm)	CO_2 uptake at 1 bar & 25 °C (mmol/g)	N_2 uptake at 1 bar & 25 °C (mmol/g)
Part I: Effect of Temperature	NHU-100	100	1.0 : 1.25	1.0 : 0.75	1105	0.47	1.76	2.58	0.17
	NHU-120	120	1.0 : 1.25	1.0 : 0.75	1118	0.49	1.73	3.32	0.10
	NHU-140	140	1.0 : 1.25	1.0 : 0.75	1013	0.44	1.74	2.85	0.12
Part II: Effect of Ligand	NHU-1	120	1.0 : 1.0	1.0 : 0.75	1254	0.54	1.72	3.11	0.25
	NHU-1.25	120	1.0 : 1.25	1.0 : 0.75	1118	0.49	1.73	3.32	0.10
	NHU-1.5	120	1.0 : 1.5	1.0 : 0.75	1067	0.45	1.74	2.51	0.19
Part III: Effect of Modulator	NHU-0.5	120	1.0 : 1.25	1.0 : 0.5	1091	0.47	1.72	2.56	0.13
	NHU-0.75	120	1.0 : 1.25	1.0 : 0.75	1118	0.49	1.73	3.32	0.10
	NHU-1*	120	1.0 : 1.25	1.0 : 1.0	1128	0.50	1.76	2.73	0.14
Part IV: Final results	NH_2-UiO-66	120	1.0 : 1.25	1.0 : 0.75	1118	0.49	1.73	3.32	0.10
	UiO-66	120	1.0 : 1.25	1.0 : 0.75	1401	0.61	1.75	2.58	0.44

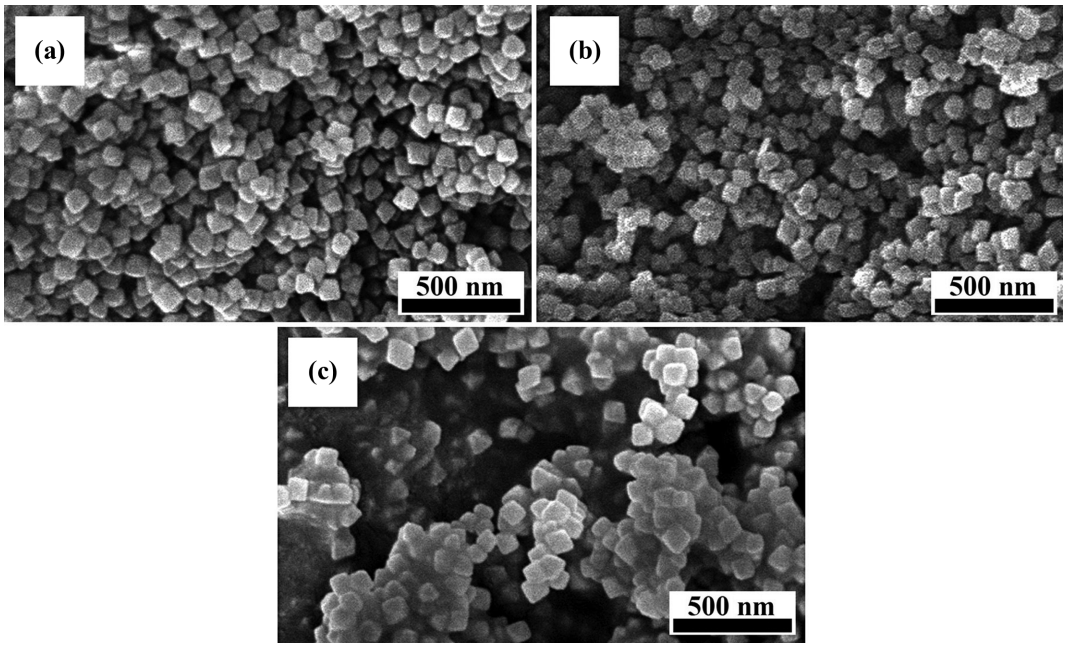


Fig. 1. FESEM micrographs of NH_2-UiO-66 synthesized at (a) 100, (b) 120 and (c) 140 °C.

NHU-100 sample, it is clear that the angles are a bit undistinguishable compared to Fig. 1(b). Moreover, when the temperature was increased to 140 °C agglomeration occurred, which is clearly obvious from Fig. 1(c).

IAST method was applied to determine the ability of these samples in separation of CO_2 from N_2. Results revealed that NHU-120 has the highest selectivity (120) compared to NHU-100 and NHU-140 that were equal to 90 and 45, respectively. This finding confirms assumptions and obtained results around BET surface area reported in Table 1.

1-2. Effect of Ligand to Metal Salt (S : L) Molar Ratio

To evaluate the effect of ligand to metal salt molar ratio, three different values (1.0, 1.25 and 1.5) were used in the synthesis of NH_2-UiO-66, and subsequently CO_2/N_2 selectivity was investigated in each case. With this regard, 0.174, 0.217, and 0.260 g NH_2-BDC were added to the synthesis solution and NH_2-UiO-66 was synthesized based on reported methodology (Sec. 2.2.1) at 120 °C. All samples were characterized using BET analysis and results are summarized in Table 1 (Part II). As can be seen from the second part of Table 1, NHU-1 has the highest S_{BET} in comparison to NHU-1.25

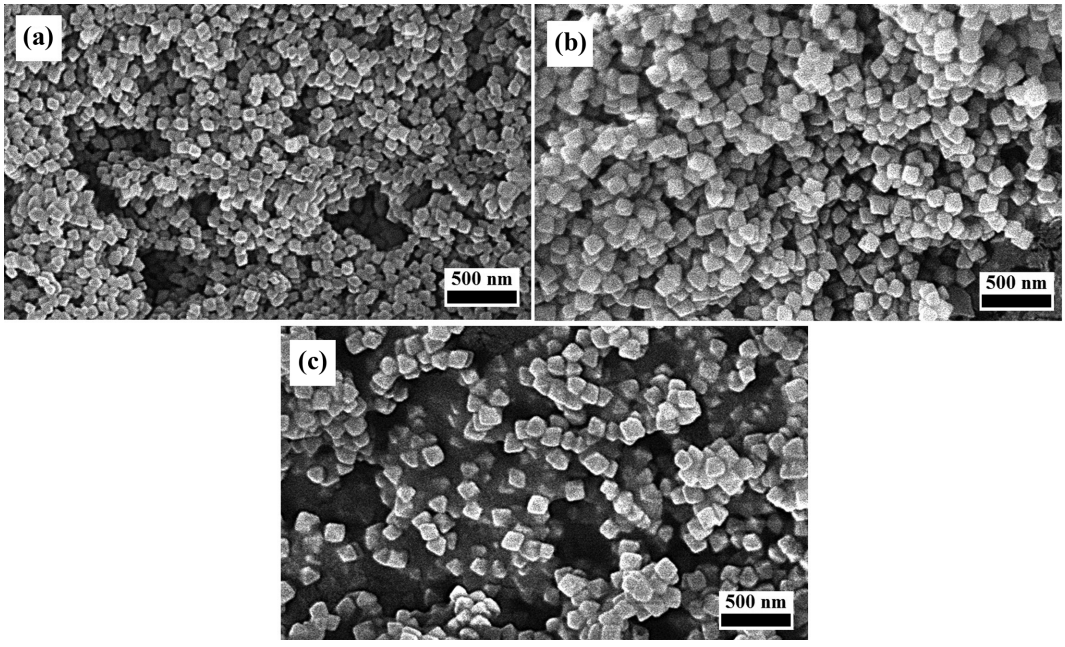


Fig. 2. FESEM micrographs of NH_2-UiO-66 synthesized with different S : L molar ratio (a) 1 : 1, (b) 1 : 1.25 and (c) 1 : 1.5.

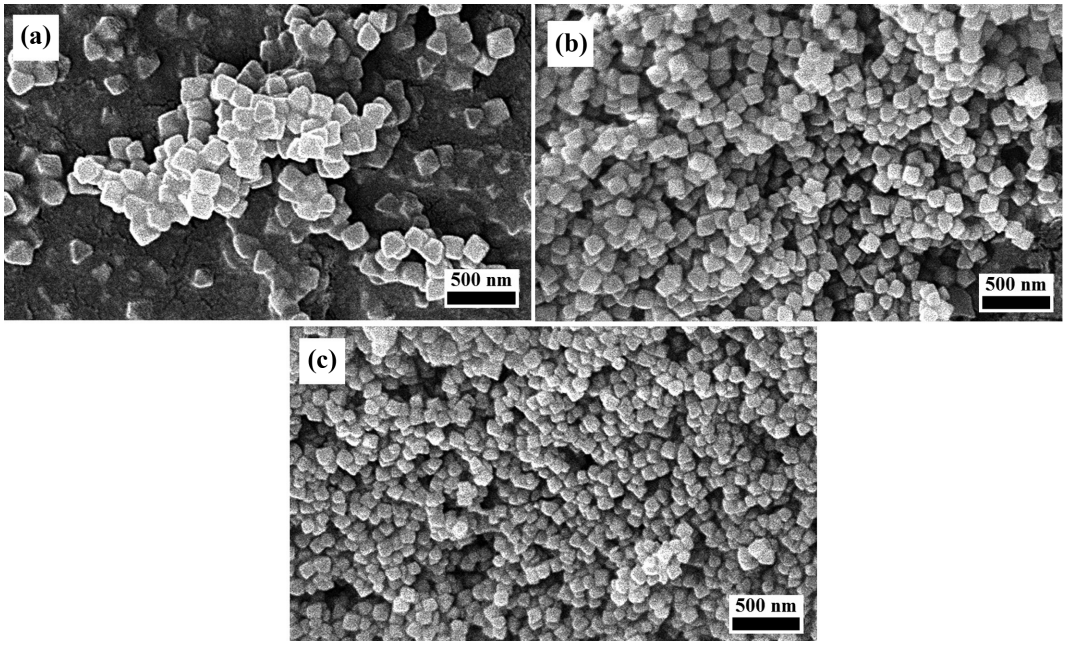


Fig. 3. FESEM micrographs of NH_2-UiO-66 synthesized with different S : M molar ratio (a) 1 : 0.5, (b) 1 : 0.75 and (c) 1 : 1.

and NHU-1.5 samples. Besides, by comparing FESEM images of Fig. 2, it is clear that, although increasing the amount of S : L molar ratio from 1.0 to 1.25 (Figs. 2(a) and (b)) did not alter the NH_2-UiO-66 morphology considerably, increasing this parameter to 1.5 clearly suppressed the formation of ideal UiO-66 crystals (Fig. 2(c)).

Findings from BET analysis were in contrast with IAST results where NHU-1.25 revealed higher CO_2/N_2 selectivity (120) compared to other samples (60 and 25 for NHU-1 and NHU-1.5, respectively). This result can be explained by the fact that by introducing more NH_2 functional groups, part of the internal volume including central octahedral cages and triangular windows might be occupied resulting in lower surface area. On the other hand, higher CO_2 adsorption capacity and selectivity of the NHU-1.25 sample may be attributed to the adequate amount of NH_2 groups in the structure of this sample, leading to more interaction between CO_2 and amine groups. Meanwhile, increasing the linker to metal salt molar ratio or introducing excess amounts of linker would terminate the growth of NH_2-UiO-66 particles through limiting the deprotonation of ligand implemented by solvent [35]. In addition, since the amount of modulator is fixed, it would not be possible for modulator to compete with high concentration of ligand to slow down the rate of crystal formation [35,36].

1-3. Effect of Modulator to Metal Salt Molar Ratio

After determination of optimum S : L molar ratio, the effect of modulator amount on textural properties of NH_2-UiO-66 as well as its CO_2/N_2 selectivity was investigated. It is known that, during synthesis of some types of MOFs, especially Zr-MOFs, application of acid modulator can help and facilitate the crystal growth through controlling the reaction kinetics. It is assumed that modulators have two essential roles in synthesis of Zr-MOFs: (1) helping in formation of $Zr_6O_4(OH)_4$ clusters, which leads to growth of crystals, and (2) inhibiting fast precipitation of amorphous solids through slowing the rate of crystal growth [37].

To recognize the effect of modulator, different S : M molar ratios (0.5, 0.75 and 1.0) were added to the homogenized solution containing 0.223 g $ZrCl_4$ and 0.22 g NH_2-BDC. Then, the synthesis process was continued based on the protocol discussed in sec. 2.2.1. Afterward, samples were characterized by BET analysis to figure out which sample possesses better textural properties. From Table 1 (Part III), it can be understood that, raising the S : M molar ratio improves the textural properties. This may be attributed to this fact that at lower S : M molar ratio (0.5), the amount of modulator was not sufficient to slow the rate of crystal growth. This claim can also be confirmed by XRD analysis and the details about as-synthesized samples are discussed in supporting information (section 3). Fig. 3(a) shows that NHU-0.5 has intergrown crystal solids. Formation of intergrown solids could result in reduction in S_{BET} of sample NHU-0.5 as well as adsorption capacity of the adsorbent. On the other hand, increasing the amount of S : M molar ratio usually improves the crystallinity as well as porosity (Fig. 3(b) and 3(c)). Nevertheless, this may lead to increase in formation of defects in SBU of MOFs, which may cause imperfection inside crystals [38] and, consequently, it would influence adsorption capability of MOFs. Therefore, it is crucial to study CO_2/N_2 selectivity of these samples and results revealed that sample NHU-0.75 has the highest selectivity (120) in comparison to NHU-0.5 (36) and sample NHU-1* (33) samples. The result confirmed that adding more amount of modulator resulted in decrease in CO_2 adsorption (due to the formation of defects) and hence, NHU-0.75 sample demonstrated better CO_2 uptake as well as selectivity compared to NHU-1*. Therefore, amount of 0.75 was selected as optimum S:M molar ratio in synthesis of NH_2-UiO-66.

Based on obtained results from the optimization process, the optimum condition for synthesis of NH_2-UiO-66 was S : L : M molar ratios of 1.0 : 1.25 : 0.75 and temperature of 120 °C. The fourth part of Table 1 compares textural characteristics of the optimum NH_2-UiO-

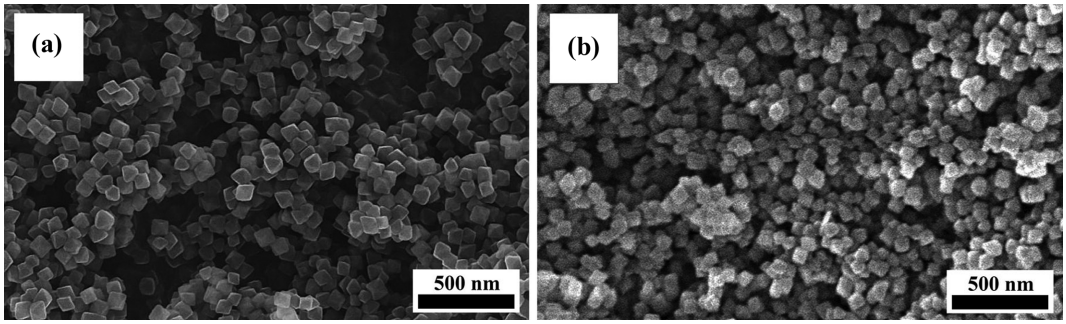


Fig. 4. FESEM micrographs of (a) UiO-66 and (b) NH_2-UiO-66.

66 and pristine UiO-66 samples. In addition, Fig. 4 compares FESEM images of UiO-66 and NH_2-UiO-66. From Fig. 4(a), the triangular-based pyramid morphology of UiO-66 particles can be observed which is completely uniform and in accordance with previous studies [9,39]. Moreover, as could be seen, after replacing the primary ligand with amine containing BDC, the morphology of NH_2-UiO-66 did not change significantly in comparison to the UiO-66 sample. However, a slight agglomeration can be observed in Fig. 4(b), which might be due to the existence of amine functional groups.

Although UiO-66 showed higher specific surface area, however, its CO_2/N_2 selectivity was much lower (10) than its aminated one (120). The main difference in textural properties of NH_2-UiO-66 and UiO-66 lies in their total pore volumes, which was reduced significantly in aminated sample. Generally, to achieve maximum adsorption capacity, it is necessary to have access to the pores of MOF. UiO-66 has rather small pores which include narrow triangular windows with pore diameter of 6 Å, octahedral and tetrahedral cavities with diameter of 11 and 8 Å, respectively [40]. When the BDC ligand is substituted by NH_2-BDC, the mentioned pore volume was reduced (20% on average) due to the presence of amine group on the linker, which may cause loss in intraparticle voids in the micropore regime as well as potentially confined diffusion. As can be observed from Table 1, this would also affect the N_2 adsorption on the MOF since the sole mechanism of nitrogen adsorption in both pristine and aminated samples is diffusion through the pores [41]. Meanwhile, N_2 is non-reactive gas molecules which could not interact with amine groups. On the other hand, CO_2 has small molecule size, higher quadrupole moment and polarizability in comparison to N_2. CO_2 is considered as a polar and Lewis acidic gas and can interact with NH_2 groups as a Lewis basic site [9]. All above-mentioned reasons justify why N_2 molecules unlike CO_2 molecules showed lower adsorption capacity (Table 1).

To have better understanding about the adsorption capacity of as-synthesized NH_2-UiO-66, CO_2 and N_2 adsorption on mentioned MOFs were implemented at 25 °C and the results are illustrated in supporting information (Fig. S1).

2. Effect of NH_2-BDC Ligand on CO_2/N_2 Selectivity of Cu_3BTC_2

$Cu_3(BTC)_2$ samples, synthesized by two solvothermal and electrochemical methods, were compared from the viewpoint of BET surface area and CO_2 adsorption capacity as well. Results demonstrated that $Cu_3(BTC)_2$ synthesized through electrochemical approach had the BET surface area of 1,627 m^2/g and CO_2 adsorption capacity of 4.4 mmol/g at 25 °C and pressure of 1 bar. These values were higher than those obtained from solvothermal method (1,306 m^2/g and 3.2 mmol/g) [32]. Therefore, electrochemical technique was chosen for synthesis of NH_2-$Cu_3(BTC)_2$.

Table 2. Effect of different weight percent of NH_2-BDC on textural properties NH_2-$Cu_3(BTC)_2$

Sample	NH_2-BDC (wt%)	S_{BET} (m^2/g)	Pore volume (cm^3/g)	Average pore diameter (nm)
NHCu-10	10	1455	0.66	1.81
NHCu-20	20	1303	0.59	1.81
NHCu-25	25	1205	0.56	1.95
Pristine	-	1627	0.69	1.69

NH_2-$Cu_3(BTC)_2$ based MOFs synthesized electrochemically with different weight percentage of NH_2-BDC, were almost similar in terms of color to the original one (dark blue). The BET analysis was carried out to evaluate the effect of adding aminated ligand to the structure of $Cu_3(BTC)_2$ and results are shown in Table 2. Note that the term "Pristine" refers to the $Cu_3(BTC)_2$ sample synthesized electrochemically without any amount of NH_2-BDC linkers within the primary synthesis solution.

As can be seen from Table 2, by adding more NH_2-BDC, the specific surface area and total pore volume decreased, while the average pore diameter increased compared to the pristine $Cu_3(BTC)_2$. Since in this study amine was incorporated in the MOF structure by using amine containing ligand rather than amine surface modification, the interior voids were partially occupied only by NH_2 groups and this could justify diminishing of the pore volumes. This observation was also reported by Ghaffari Nik et al. [30] who observed a reduction in the surface area and total pore volume of NH_2-$Cu_3(BTC)_2$ after substitution of part of BTC ligand with NH_2-BDC one. They confirmed that this reduction is attributed to the presence of primary amine group that partially occupied the micropores of NH_2-$Cu_3(BTC)_2$.

Similarly, to understand the performance of each aminated sample toward CO_2 separation from N_2, single component adsorption experiments were carried out for all samples (Fig. 5). Among synthesized aminated $Cu_3(BTC)_2$, the NHCu-20 sample showed the highest CO_2/N_2 selectivity (53) in comparison to NHCu-10 and NHCu-25 samples with CO_2/N_2 selectivity of 23 and 22, respectively. From Fig. 5 it is clear that adding amine groups could result in reduction of CO_2 uptake compared to the pristine sample. How-

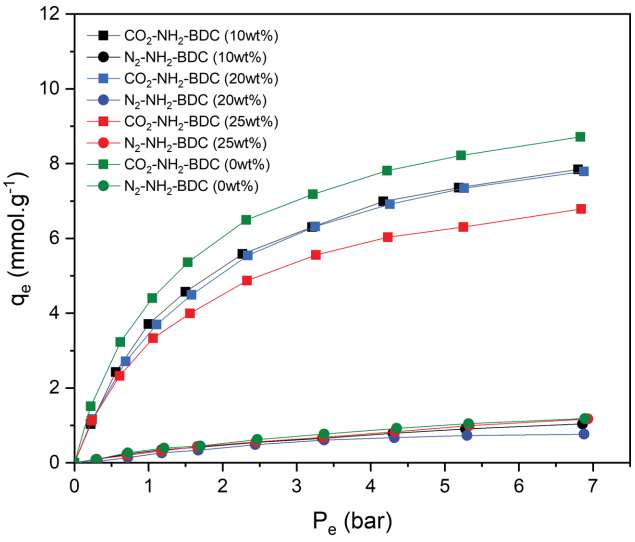


Fig. 5. CO_2 and N_2 adsorption on NH_2-$Cu_3(BTC)_2$ with different weight percent of NH_2-BDC.

ever, for the NH_2-BDC (20 wt%) sample no significant change was observed compared to NH_2-BDC (10 wt%). Since it was presumed that adding more aminated ligand might lead to increase in CO_2 adsorption; interestingly, no significant change was observed in CO_2 adsorption behavior. This inconsistency in CO_2 affinity can be attributed to the presence of NH_2 groups that might make more carbamates with CO_2, which improves CO_2 separation and prevents further CO_2 reduction [42]. In addition, there was a reduction in nitrogen adsorption after adding aminated ligand to 20 wt%, which led to an increase in the CO_2/N_2 selectivity. Meanwhile, further increase in NH_2-BDC to 25 wt% caused a reduction in CO_2 adsorption capacity associated with an increase in nitrogen adsorption capacity, leading to a drop in the CO_2/N_2 selectivity. This observation can be interpreted from two different chemical and physical view of points. On one hand, by exchanging one BTC molecule with NH_2-BDC, one carboxylate group (out of three) of a linker is substituted by one amine containing aromatic ring. This may bring distortion in paddle-wheel structure of $Cu_3(BTC)_2$ and a gap may be created between copper dimmer and linker molecule. As the amount of NH_2 increased, the coordination number of copper atoms was decreased, and this caused remaining a positive charge in the structure. Therefore, positive charge might be compensated by nitrogen species [43]. Besides, the compensation of positive charge would take place through interaction between copper atom and electron donor atom (i.e., amine group) and consequently, CO_2 would not get the chance to interact with amine groups. Therefore, the more amount of NH_2-BDC linker, the less open metal sites seem to be available for CO_2 gas molecules [44]. On the other hand, increasing the amount of amine containing ligand causes reduction in total pore volume and, more importantly, increase of average pore diameter which allows nitrogen molecules compete more easily with CO_2 molecule for diffusion to the adsorbent pores in comparison to pristine sample. To sum up, this occurrence leads to decrease in CO_2 adsorption capacity of NH_2-$Cu_3(BTC)_2$.

$Cu_3(BTC)_2$ octahedral particles are clearly shown in Fig. 6(a). However, using mixed ligand (20 wt% NH_2-BDC) distorted the appearance of the particles considerably (Fig. 6(b)). This can be attributed to replacement of a part of trimesic acid (BTC) with NH_2-BDC that caused whisker-like roughness on the surface of crystals, which was previously reported in literature [30,42].

Preserving the crystalline structure of MOF is an important principle that must be considered in synthesis of functionalized MOFs. In this regard, XRD analysis of both types of MOFs was implemented and their spectra are shown in Fig. 7.

The intact XRD spectra of UiO-66 and $Cu_3(BTC)_2$ before and after NH_2-BDC linker exchange (Fig. 7) demonstrated that amination did not change the primary crystal structure. This can be proved by the justification that the locations and intensities of peaks did not vary after using amine groups in synthesis procedure.

Results of other complementary characterizations associated with as-synthesized products (FTIR and TGA) are given in supplementary information for review. According to FTIR analysis of pristine UiO-66, $Cu_3(BTC)_2$ and their amine containing moieties (Fig. S3), the presence of amine groups could be confirmed based on discrepancy in formation of relevant peaks. Besides, comparing TGA

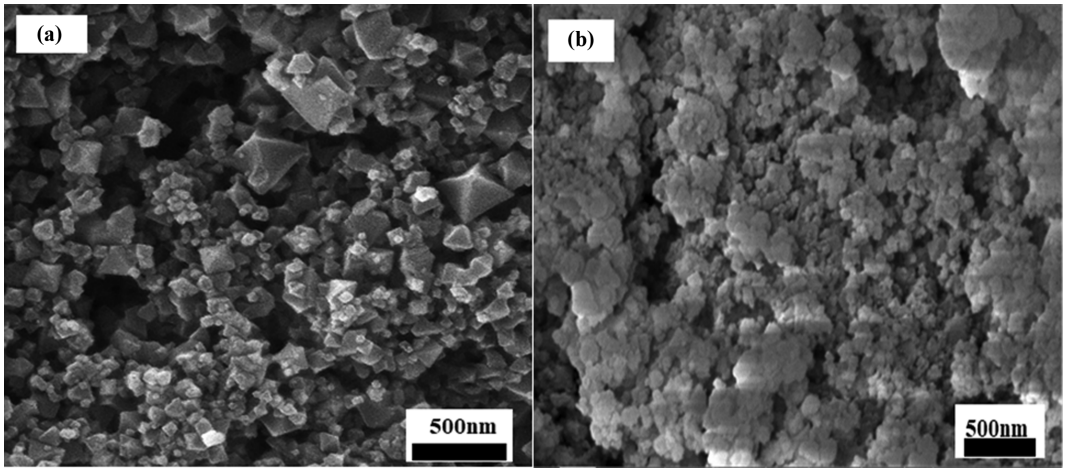


Fig. 6. FESEM micrographs of (a) $Cu_3(BTC)_2$ and (b) NH_2-$Cu_3(BTC)_2$.

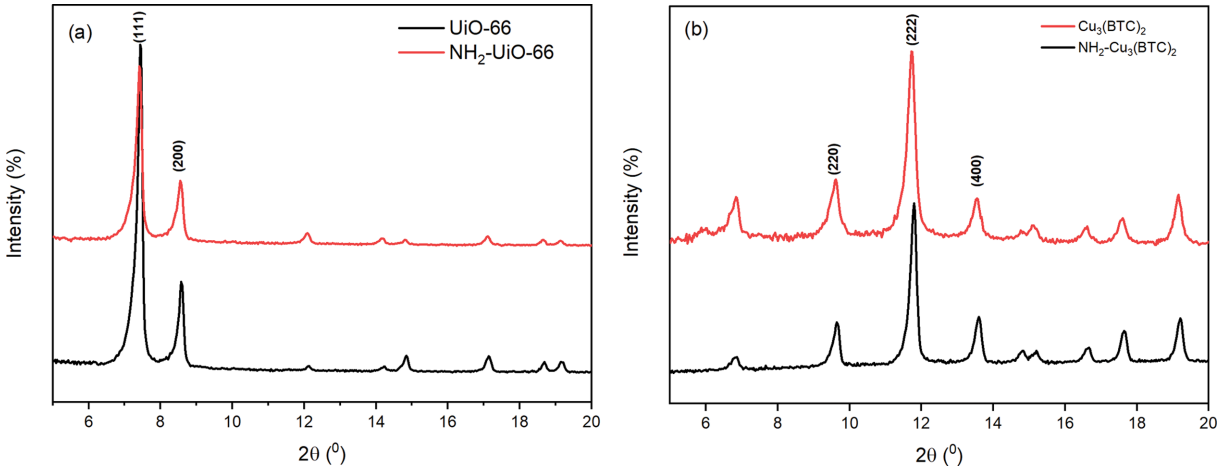


Fig. 7. XRD patterns of pristine and aminated form of (a) UiO-66 and (b) $Cu_3(BTC)_2$.

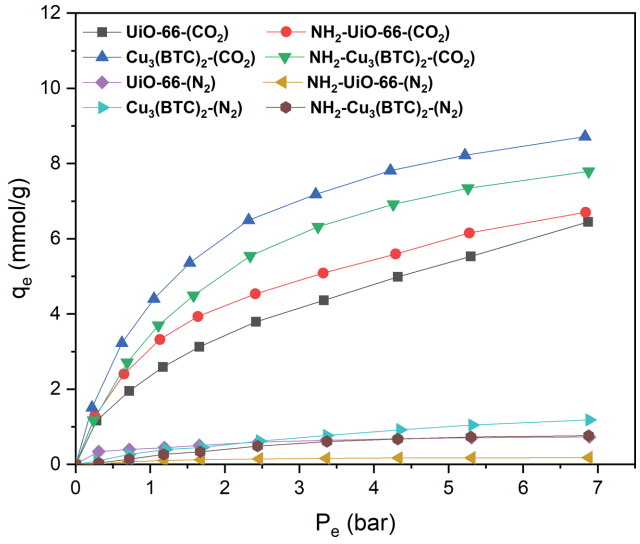


Fig. 8. CO_2 and N_2 adsorption capacity of UiO-66, $Cu_3(BTC)_2$ and their optimized aminated derivatives at 25 °C.

analysis of as-synthesized samples (Fig. S4) revealed that linker exchange in UiO-66 brought drastic reduction in thermal stability of UiO-66 rather than $Cu_3(BTC)_2$.

3. Comparative Study of As-synthesized MOFs Performances

Fig. 8 shows CO_2 and N_2 adsorption capacity of UiO-66, $Cu_3(BTC)_2$ and their aminated derivatives (optimum condition) at 25 °C in the pressure range of 0-7 bar. Since CO_2 has smaller molecule, higher quadrupole moment and is more polarizable than N_2, it would be adsorbed more preferentially on as-synthesized MOFs. From Fig. 8, it is clear that pristine $Cu_3(BTC)_2$ had the highest CO_2 capacity, while pristine UiO-66 had the lowest. Since both pristine MOFs possess CUS, this finding might be attributed to lower BET surface area and consequently fewer available active sites (such as octahedral cages) of UiO-66. These active sites, which are usually located inside the pores, play the hosting role for guest molecules and the adsorption process will take place by occupation of these vacant sites. As long as the pore diameter of UiO-66 was wider compared to $Cu_3(BTC)_2$, the role of porosity or size exclusion mechanism was less effective during adsorption process [37]. Therefore, lower CO_2 adsorption in pristine UiO-66 would enhance the competition between CO_2 and N_2 molecules for occupying vacant sites, which results in lower CO_2/N_2 selectivity.

In the case of NH_2-UiO-66, higher CO_2 adsorption in comparison to pristine UiO-66 could be attributed to reversible selective chemical reaction between CO_2 and NH_2 groups. This reaction follows carbamate zwitterion mechanism which was first proposed by Caplow [45] and Danckwerts [46]:

$$CO_2 + RNH_2 \rightleftharpoons RNH_2^+COO^- \quad (1)$$

$$NH_2 + COO^- + RNH_2 \rightleftharpoons RNHCOO^- + RNH_3^+ \quad (2)$$

In the first reaction, one CO_2 molecule reacts with one amine molecule to produce zwitterion intermediate and then the carbamate ion would be formed after another deprotonation by a secondary amine. Therefore, while chemisorption would be the dominant mechanism for CO_2 adsorption, N_2 is physically adsorbed due to its non-reactive nature [47]. This difference in adsorption mechanisms enhances the CO_2/N_2 selectivity in NH_2-UiO-66. Meanwhile, unlike what happened for NH_2-$Cu_3(BTC)_2$, replacing BDC with NH_2-BDC does not bring either distortion or defect to crystalline structure of Zr-MOF. Therefore, there would be no interaction between amine group and CUS, and the polar functional groups are available only for CO_2 molecules and increase in CO_2 adsorption would be a certain consequence. Carbamate zwitterion mechanism was also correct about CO_2 adsorption on NH_2-$Cu_3(BTC)_2$. However, as stated before (sec. 3.4), the adsorption capacity decreased after utilizing functionalized linker in the structure of $Cu_3(BTC)_2$. Table 3 summarizes CO_2 and N_2 adsorption capacity of as-synthesized MOFs (at 25 °C and 1 bar) as well as their calculated CO_2/N_2 selectivity using IAST methodology.

Enhancement in CO_2/N_2 selectivity is not just limited to chemical reactions between CO_2 molecules and amine groups. Reduction in N_2 adsorption is another important reason which can be discussed from two different point of views: I) Physical and chemical aspects: In general, probability for nitrogen molecules with larger

Table 3. CO_2 and N_2 adsorption capacity of as-synthesized MOFs and their selectivity at 1 bar and 25 °C

MOF	BET (m^2/g)	CO_2 uptake (mmol/g)	N_2 uptake (mmol/g)	CO_2/N_2 selectivity	Pore volume (cm^3/g)	Average pore diameter (nm)
NH_2-UiO-66	1254	3.32	0.11	120	0.49	1.73
NH_2-$Cu_3(BTC)_2$	1242	3.86	0.24	53	0.59	1.81
UiO-66	1401	2.32	0.73	10	0.61	1.75
$Cu_3(BTC)_2$	1627	4.40	0.37	33	0.69	1.69

Table 4. A comparative study about CO_2 adsorption between previous and current studies

MOF	Synthesis method	BET (m^2/g)	Temp. (°C)	Pressure (bar)	CO_2 uptake (mmol/g)	Ref.
NH_2-UiO-66	Solvothermal	1258	25	1	3.20	[9]
NH_2-UiO-66	Solvothermal	1220	23	1	2.86	[48]
NH_2-UiO-66	Solvothermal	842	25	1	1.10	[49]
NH_2-UiO-66	Microwave	1118	25	1	3.50	[34]
NH_2-UiO-66	Solvothermal	1123	25	1	3.00	[50]
NH_2-UiO-66	Solvothermal	826	35	1	1.64	[30]
NH_2-$Cu_3(BTC)_2$	Solvothermal	650	35	1	1.84	[30]
NH_2-$Cu_3(BTC)_2$	Solvothermal	797	35	1	0.82	[42]
UiO-66-NO_2-NH_2	Solvothermal	868	23	1	2.68	[51]
NH_2-UiO-66	Solvothermal	1254	25	1	3.32	This study
NH_2-$Cu_3(BTC)_2$	Electrochemical	1242	25	1	3.86	This study
UiO-66	Solvothermal	1401	25	1	2.32	This study
$Cu_3(BTC)_2$	Electrochemical	1627	25	1	4.40	This study

kinetic diameter (0.365 nm) to pass through adsorbent pores is smaller than CO_2 with kinetic diameter 0.330 nm. Besides, nitrogen molecules possess lower quadrupole moment and polarizability as opposed to CO_2 molecules. This leads to a weaker interaction between nitrogen molecules and CUS than CO_2 molecules. Therefore, in comparison to CO_2 adsorption capacity, MOF would definitely adsorb lower amount of nitrogen molecules. II) Textural properties of MOF: When functional groups are incorporated in an MOF structure (in this study "amine group") the accessible spaces as well as vacant active sites for guest molecules will be confined. This restriction in adsorption becomes more significant with an increase in concentration of functional groups. This fact can be proved by looking at textural properties of as-synthesized MOFs given in Tables 1 and 2 (compare total pore volume for pristine and aminated MOFs). In general, this limitation exists for both gases; however, it is more crucial for nitrogen molecules, which is completely a nonreactive and neutral gas and is rejected more in the presence of amine groups [9]. This reduction in nitrogen adsorption will improve CO_2/N_2 selectivity, which is the main objective of the present study.

To throw some light on the performance of as-synthesized samples in this research, Table 4 presents results of some studies concerning with CO_2 adsorption and separation. As one can see, the amount of CO_2 storage obtained by NH_2-UiO-66 in this study is among the highest values that have been reported so far for this type of MOF via solvothermal method. This is also true about NH_2-$Cu_3(BTC)_2$ in which there is no report about CO_2 adsorption capacity higher than the recorded amount of this study.

4. Isosteric Heat of Adsorption

To evaluate the interaction between the adsorbent surface and guest molecules, isosteric heat of adsorption has to be considered as an important thermodynamic parameter [52]. The isosteric heat of adsorption presented by Clausius-Clapeyron is defined as follows:

$$Q_{st} = RT^2\left(\frac{\partial \ln P}{\partial T}\right) \tag{3}$$

Since the Langmuir isotherm model fitted the equilibrium data with reasonable accuracy, the temperature-dependent form of this model was used for calculation of heat of adsorption. Substituting temperature-dependent constants of the Langmuir equation in the original formula, the Langmuir isotherm model becomes the following equation [53]:

$$q = \frac{K_{L0}\exp\left(\frac{Q}{RT}\right)q_0\exp(\delta(T-T_0))P}{1+K_{L0}\exp\left(\frac{Q}{RT}\right)P} \tag{4}$$

where q_0 is the adsorption capacity (mmol/g) at reference temperature which was assumed to be 298 K, δ is a parameter which is related to expansion coefficient (1/K). From thermodynamic point of view, thermal expansion coefficient explains the tendency of matter to change in volume with respect to alteration in temperature. To be more specific, when a substance is heated, it enhances the kinetic energy, which results in increase in vibration and movement of molecules [54]. K_{L0} is the adsorption affinity at reference temperature (L/mmol) and Q is the heat of adsorption at zero coverage (J/mol). Fig. 9 illustrates the behavior of equilibrium data which were fitted by temperature dependent form of Langmuir isotherm model at 25, 35 and 45 °C and constants are listed in Table 5.

The isosteric heat of adsorption can be obtained through sub-

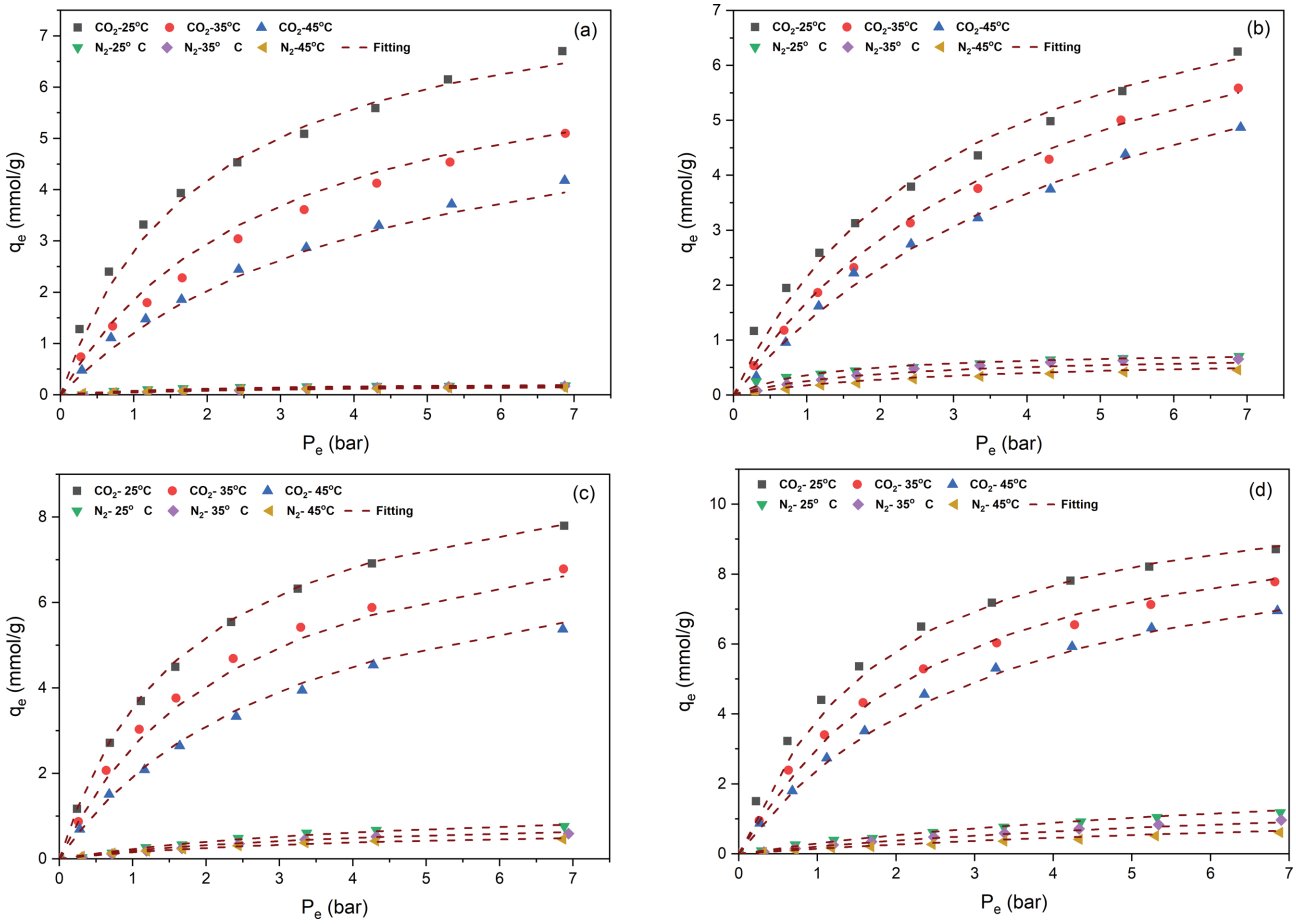


Fig. 9. Adsorption isotherms of CO_2 and N_2 on (a) NH_2-UiO-66, (b) UiO-66, (c) NH_2-$Cu_3(BTC)_2$ and (d) $Cu_3(BTC)_2$ at three different temperatures. Closed symbols represent experimental data and dashed lines denote fitting with temperature dependent Langmuir model.

Table 5. Temperature-dependent Langmuir model constants for CO_2 adsorption on MOFs

Sample	Constants	CO_2
NH_2-UiO-66	q_0 (mmol/g)	8.445
	δ (K^{-1})	0.01301
	K_{L0} (L/mmol)	1.86E-5
	Q (J/mol)	46050
	R^2	0.989
UiO-66	q_0 (mmol/g)	8.892
	δ (K^{-1})	0.00017
	K_{L0} (L/mmol)	2.43E-5
	Q (J/mol)	32462
	R^2	0.992
NH_2-$Cu_3(BTC)_2$	q_0 (mmol/g)	9.844
	δ (K^{-1})	0.00975
	K_{L0} (L/mmol)	4.913E-5
	Q (J/mol)	54251
$Cu_3(BTC)_2$	q_0 (mmol/g)	10.885
	δ (K^{-1})	0.00041
	K_{L0} (L/mmol)	3.15E-5
	Q (J/mol)	34149
	R^2	0.989

stitution of temperature dependent form of Langmuir model into Eq. (4):

$$Q_{st} = Q - \frac{m\delta}{1-\theta} \quad (5)$$

where Q and δ are obtained through fitting the temperature-dependent form of Langmuir isotherm model, m is the product of R, and T^2 and θ is the fractional loading expressed by q/q_{max}. From Fig. 10, it can be deduced that changing adsorption temperature does not affect isosteric heat of adsorption of all samples, which proves that the enthalpy of adsorption is temperature independent. Although the temperature used for thermodynamic analysis was in a narrow range, it was recognized by Armstrong et al. that for wider range of temperature, 280 to 350 K, the isosteric heat of adsorption remains unchanged [55]. Note that gas separation processes involving higher temperatures are impractical.

It can be seen that aminated MOFs showed higher Q_{st} for CO_2 as opposed to the parental ones. This is in accordance with the mentioned justification that the existence of amine groups increases the interaction between the adsorbent and CO_2 and also causes a chemical reaction, which ultimately raises the Q_{st} for CO_2. Among all samples, NH_2-$Cu_3(BTC)_2$ showed the highest isosteric heat of adsorption with 43 kJ/mol in comparison to $Cu_3(BTC)_2$ (33 kJ/

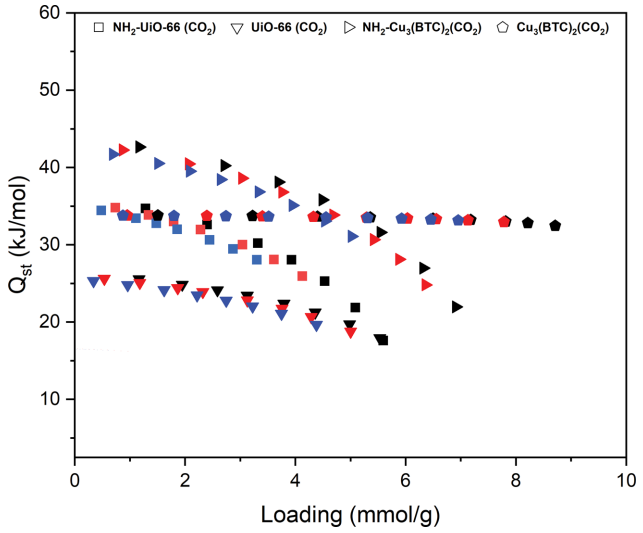


Fig. 10. Isosteric heat of adsorption of CO_2 on parental and aminated derivatives of UiO-66 and $Cu_3(BTC)_2$ at three different temperatures. Black, red and blue colors represent heat of adsorption at 25, 35 and 45 °C, respectively.

mol), UiO-66 (25.6 kJ/mol) and NH_2-UiO-66 (34.7 kJ/mol), which was in accordance with similar studies in which they applied NH_2-BDC linker as a ligand [22,56-59].

High isosteric heat of adsorption (>60 kJ·mol^{-1}) can occur in liquid phase where CO_2 easily diffuses through amine solution and strongly reacts with amine to form carbamate. In the solid phase, CO_2 should diffuse through the pores of a porous solid (MOF), which occurs with much slower rate compared to liquid phase. The lower of CO_2 diffusion leads to weaker reaction with amine and therefore lower rate of carbamate formation. Hence, the isosteric heat of adsorption remains lower than the value normally needed for carbamate formation. In addition, as loading increases, a relatively high heat of adsorption accompanied by relative sharp drop can be observed, which is attributed to presence of dipole moment of amine group which provides strong adsorption sites [50].

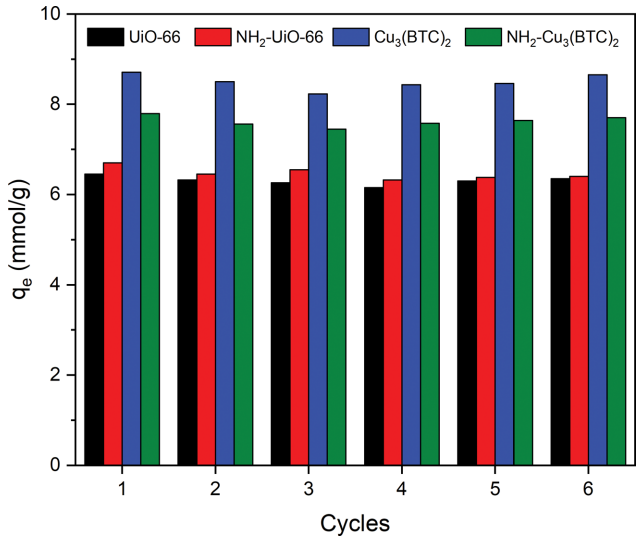


Fig. 11. Cyclic adsorption/desorption of CO_2 on UiO-66, NH_2-UiO-66, $Cu_3(BTC)_2$ and NH_2-$Cu_3(BTC)_2$.

5. Cyclic Adsorption/Desorption

For long-term operation, it is necessary to evaluate the stability of the adsorbent in keeping its adsorption capacity during several adsorption-desorption cycles. If the adsorbent loses its durability in a few sequential cycles, it would not be recommended even for application in pilot scale. As matter of fact, this idea is indeed independent of scale. Fig. 11 illustrates adsorption/desorption of CO_2 on UiO-66, NH_2-UiO-66, $Cu_3(BTC)_2$ and NH_2-$Cu_3(BTC)_2$ for six sequential cycles. For this purpose, the adsorption process was carried out at 25 °C under pressure range of 0.5-7 bar, while, for desorption process the used samples were degassed at 150 °C under atmospheric pressure for 24 h. It is clear that the CO_2 adsorption capacity did not change significantly during six cycles, which proves the durability of synthesized MOFs.

CONCLUSION

NH_2-UiO-66 and NH_2-$Cu_3(BTC)_2$ were successfully synthesized through solvothermal and electrochemical methods, respectively. For NH_2-UiO-66, the effects of synthesis parameters, including synthesis temperature, ligand to metal salt molar ratio (S : L) and modulator to metal salt molar ratio (S : M) on CO_2/N_2 selectivity, were investigated. The best result was obtained at synthesis temperature of 120 °C and S : L : M molar ratio of 1 : 1.25 : 0.75 with CO_2/N_2 selectivity of 120 at 25 °C and 1 bar. NH_2-$Cu_3(BTC)_2$ containing 20 wt% NH_2-BDC showed better CO_2/N_2 separation performance (selectivity of 53) than parental $Cu_3(BTC)_2$, since the reduction of N_2 adsorption in aminated form was more considerable than the pristine one. CO_2 isosteric heat of adsorption study revealed that amine containing MOFs released higher heat of adsorption due to interaction and chemical reaction between CO_2 and NH_2 groups in the structure of MOFs. Six sequential adsorption/desorption process showed that all MOFs were steady in CO_2 adsorption for long-term operations. From this study, it can be concluded that NH_2-UiO-66 with the CO_2/N_2 selectivity of 120 could be a better candidate for CO_2 and N_2 mixture separation as opposed to NH_2-$Cu_3(BTC)_2$ with the CO_2/N_2 selectivity of 53, because the absence of distortion and defects in crystalline structure of MOF makes the functional group accessible for CO_2 molecules.

SUPPORTING INFORMATION

Additional information as noted in the text. This information is available via the Internet at http://www.springer.com/chemistry/journal/11814.

REFERENCES

1. R. Sabouni, H. Kazemian and S. Rohani, *Micropor. Mesopor. Mater.*, **175**, 85 (2013).
2. A. Sayari, Y. Belmabkhout and R. Serna-Guerrero, *Chem. Eng. J.*, **171**, 760 (2011).
3. R. Sabouni, H. Kazemian and S. Rohani, *Environ. Sci. Technol.*, **47**, 9372 (2013).

4. S. Choi, J. H. Drese and C. W. Jones, *ChemSusChem: Chem. Sustainability Energy Mater.*, **2**, 796 (2009).
5. L. Wang, Z. Liu, P. Li, J. Yu and A. E. Rodrigues, *Chem. Eng. J.*, **197**, 151 (2012).
6. T. L. Dantas, F. M. T. Luna, I. J. Silva Jr., A. E. B. Torres, D. C. de Azevedo, A. E. Rodrigues and R. F. Moreira, *Chem. Eng. J.*, **172**, 698 (2011).
7. M. Ding, R. W. Flaig, H.-L. Jiang and O. M. Yaghi, *Chem. Soc. Rev.*, **48**, 2783 (2019).
8. Z. Hu, Y. Wang, B. B. Shah and D. Zhao, *Adv. Sustainable Syst.*, **3**, 1970002 (2019).
9. H. Molavi, A. Eskandari, A. Shojaei and S. A. Mousavi, *Micropor. Mesopor. Mater.*, **257**, 193 (2018).
10. Z.-F. Pang, T.-Y. Zhou, R.-R. Liang, Q.-Y. Qi and X. Zhao, *Chem. Sci.*, **8**, 3866 (2017).
11. W. Zhou, H. Wu and T. Yildirim, *J. Am. Chem. Soc.*, **130**, 15268 (2008).
12. A. M. Khattak, Z. A. Ghazi, B. Liang, N. A. Khan, A. Iqbal, L. Li and Z. Tang, *J. Mater. Chem. A*, **4**, 16312 (2016).
13. R. C. Huxford, J. Della Rocca and W. Lin, *Curr. Opin. Chem. Biol.*, **14**, 262 (2010).
14. Q. Fang, J. Wang, S. Gu, R. B. Kaspar, Z. Zhuang, J. Zheng, H. Guo, S. Qiu and Y. Yan, *J. Am. Chem. Soc.*, **137**, 8352 (2015).
15. H. Chen, Y. Liu, T. Cai, W. Dong, L. Tang, X. Xia, L. Wang and T. Li, *ACS Appl. Mater. Interfaces*, **11**, 28791 (2019).
16. S. Lin, C. S. Diercks, Y.-B. Zhang, N. Kornienko, E. M. Nichols, Y. Zhao, A. R. Paris, D. Kim, P. Yang and O. M. Yaghi, *Science*, **349**, 1208 (2015).
17. S. Dalapati, S. Jin, J. Gao, Y. Xu, A. Nagai and D. Jiang, *J. Am. Chem. Soc.*, **135**, 17310 (2013).
18. B. Assfour and G. Seifert, *Micropor. Mesopor. Mater.*, **133**, 59 (2010).
19. H. Wang, D. Jiang, D. Huang, G. Zeng, P. Xu, C. Lai, M. Chen, M. Cheng, C. Zhang and Z. Wang, *J. Mater. Chem. A*, **7**, 22848 (2019).
20. H. Wang, Z. Zeng, P. Xu, L. Li, G. Zeng, R. Xiao, Z. Tang, D. Huang, L. Tang and C. Lai, *Chem. Soc. Rev.*, **48**, 488 (2019).
21. S. Xian, Y. Wu, J. Wu, X. Wang and J. Xiao, *Ind. Eng. Chem. Res.*, **54**, 11151 (2015).
22. Z. H. Rada, H. R. Abid, J. Shang, Y. He, P. Webley, S. Liu, H. Sun and S. Wang, *Fuel*, **160**, 318 (2015).
23. R. Ben-Mansour, M. Habib, O. Bamidele, M. Basha, N. Qasem, A. Peedikakkal, T. Laoui and M. Ali, *Appl. Energy*, **161**, 225 (2016).
24. M. Kim and S. M. Cohen, *CrystEngComm*, **14**, 4096 (2012).
25. J. B. DeCoste, G. W. Peterson, B. J. Schindler, K. L. Killops, M. A. Browe and J. J. Mahle, *J. Mater. Chem. A*, **1**, 11922 (2013).
26. M. R. Azhar, H. R. Abid, V. Periasamy, H. Sun, M. O. Tade and S. Wang, *J. Colloid Interface Sci.*, **500**, 88 (2017).
27. M. Kandiah, M. H. Nilsen, S. Usseglio, S. Jakobsen, U. Olsbye, M. Tilset, C. Larabi, E. A. Quadrelli, F. Bonino and K. P. Lillerud, *Chem. Mater.*, **22**, 6632 (2010).
28. Y. Yang, P. Shukla, S. Wang, V. Rudolph, X.-M. Chen and Z. Zhu, *Rsc Adv.*, **3**, 17065 (2013).
29. B. Seoane, J. Coronas, I. Gascon, M. E. Benavides, O. Karvan, J. Caro, F. Kapteijn and J. Gascon, *Chem. Soc. Rev.*, **44**, 2421 (2015).
30. O. G. Nik, X. Y. Chen and S. Kaliaguine, *J. Membr. Sci.*, **413**, 48 (2012).
31. F. Wu, L. Lin, H. Liu, H. Wang, J. Qiu and X. Zhang, *J. Membr. Sci.*, **544**, 342 (2017).
32. K. Esfandiari, A. A. Ghoreyshi and M. Jahanshahi, *Ind. Eng. Chem. Res.*, **56**, 14610 (2017).
33. K. Pirzadeh, A. A. Ghoreyshi, M. Rahimnejad and M. Mohammadi, *Korean J. Chem. Eng.*, **35**, 974 (2018).
34. A. Huang, L. Wan and J. Caro, *Mater. Res. Bull.*, **98**, 308 (2018).
35. B. Shan, J. B. James, M. R. Armstrong, E. C. Close, P. A. Letham, K. Nikkhah, Y. Lin and B. Mu, *J. Phys. Chem. C*, **122**, 2200 (2018).
36. S. M. Chavan, G. C. Shearer, S. Svelle, U. Olsbye, F. Bonino, J. Ethiraj, K. P. Lillerud and S. Bordiga, *Inorg. Chem.*, **53**, 9509 (2014).
37. Z. Hu, I. Castano, S. Wang, Y. Wang, Y. Peng, Y. Qian, C. Chi, X. Wang and D. Zhao, *Cryst. Growth Des.*, **16**, 2295 (2016).
38. G. C. Shearer, S. Chavan, J. Ethiraj, J. G. Vitillo, S. Svelle, U. Olsbye, C. Lamberti, S. Bordiga and K. P. Lillerud, *Chem. Mater.*, **26**, 4068 (2014).
39. M. Jia, Y. Feng, S. Liu, J. Qiu and J. Yao, *J. Membr. Sci.*, **539**, 172 (2017).
40. A. M. Ploskonka and J. B. DeCoste, *ACS Appl. Mater. Interfaces*, **9**, 21579 (2017).
41. G. W. Peterson, J. B. DeCoste, F. Fatollahi-Fard and D. K. Britt, *Ind. Eng. Chem. Res.*, **53**, 701 (2014).
42. B. Ge, Y. Xu, H. Zhao, H. Sun, Y. Guo and W. Wang, *Materials*, **11**, 1421 (2018).
43. S. Marx, W. Kleist and A. Baiker, *J. Catal.*, **281**, 76 (2011).
44. F. Martínez, R. Sanz, G. Orcajo, D. Briones and V. Yángüez, *Chem. Eng. Sci.*, **142**, 55 (2016).
45. M. Caplow, *J. Am. Chem. Soc.*, **90**, 6795 (1968).
46. P. Danckwerts, *Chem. Eng. Sci.*, **34**, 443 (1979).
47. E. Stavitski, E. A. Pidko, S. Couck, T. Remy, E. J. Hensen, B. M. Weckhuysen, J. Denayer, J. Gascon and F. Kapteijn, *Langmuir*, **27**, 3970 (2011).
48. H. R. Abid, J. Shang, H.-M. Ang and S. Wang, *Int. J. Smart Nano Mater.*, **4**, 72 (2013).
49. M. Vahidi, A. M. Rashidi and A. Tavasoli, *J. Iranian Chem. Soc.*, **14**, 2247 (2017).
50. G. E. Cmarik, M. Kim, S. M. Cohen and K. S. Walton, *Langmuir*, **28**, 15606 (2012).
51. Z. H. Rada, H. R. Abid, H. Sun and S. Wang, *J. Chem. Eng. Data*, **60**, 2152 (2015).
52. L. Mei, T. Jiang, X. Zhou, Y. Li, H. Wang and Z. Li, *Chem. Eng. J.*, **321**, 600 (2017).
53. V. Maramis, A. Kurniawan, A. Ayucitra, J. Sunarso and S. Ismadji, *Front. Chem. Sci.* Eng., **6**, 58 (2012).
54. Q. Guo, *Thermosets: structure, properties, and applications*, Woodhead Publishing Limited, 65 (2012).
55. M. R. Armstrong, B. Shan, Z. Cheng, D. Wang, J. Liu and B. Mu, *Chem. Eng. Sci.*, **167**, 10 (2017).
56. Y. Cao, H. Zhang, F. Song, T. Huang, J. Ji, Q. Zhong, W. Chu and Q. Xu, *Materials*, **11**, 589 (2018).
57. Y. Yang, R. Lin, L. Ge, L. Hou, P. Bernhardt, T. E. Rufford, S. Wang, V. Rudolph, Y. Wang and Z. Zhu, *Dalton Transact.*, **44**, 8190 (2015).
58. B. Yuan, D. Ma, X. Wang, Z. Li, Y. Li, H. Liu and D. He, *Chem. Commun.*, **48**, 1135 (2012).
59. B. Arstad, H. Fjellvåg, K. O. Kongshaug, O. Swang and R. Blom, *Adsorption*, **14**, 755 (2008).

Supporting Information

CO_2 and N_2 adsorption and separation using aminated UiO-66 and $Cu_3(BTC)_2$: A comparative study

Kasra Pirzadeh, Kourosh Esfandiari, Ali Asghar Ghoreyshi†, and Mostafa Rahimnejad

Chemical Engineering Department, Babol Noshirvani University of Technology, Babol, Iran
(*Received 7 September 2019 • accepted 17 November 2019*)

1. IAST Calculation

IAST method is a technique to determine selectivity of a two-component mixture by means of data available around adsorption isotherms of its constituents [1,2]. In this research, IAST method was employed to calculate the selectivity of CO_2/N_2 (15/85 vol%) at 298 K. IAST is based on the following equation which is similar to Raoult's law in vapor/liquid equilibrium:

$$Py_i = P_i = x_i P_i^0(\pi), \qquad i=1, 2, 3, \ldots, N \tag{S1}$$

where y_i and x_i are the mole fractions of component i in the gas phase and adsorbed phase, respectively, and $P_i^0(\pi)$ is the pressure of component i at the same spreading pressure as that of the mixture. π (so-called spreading pressure) is as follow:

$$\pi = \frac{(R_g T)}{A}\int_0^{P_1^0}\frac{q_1}{P_1}dP_1 = \frac{(R_g T)}{A}\int_0^{P_2^0}\frac{q_2}{P_2}dP_2 = \ldots = \frac{(R_g T)}{A}\int_0^{P_N^0}\frac{q_N}{P_N}dP_N \tag{S2}$$

where A is the specific surface area of the adsorbent (m^2/kg), R_g is the universal gas constant (J/mol·K), T is the temperature (K), and q is the amount of adsorption (mmol/g) at pressure of P (MPa). z which is the reduced spreading pressure of the sorbed phase is as follow:

$$z = \frac{A\pi}{R_g T} = \int_0^{P_1^0(\pi)}\frac{q_1}{P_1}dP_1 = \int_0^{P_2^0(\pi)}\frac{q_2}{P_2}dP_2 = \ldots = \int_0^{P_N^0(\pi)}\frac{q_N}{P_N}dP_N \tag{S3}$$

By combination of Langmuir and IAST (Eq. (3)) models, the following equation is obtained:

$$z_i = q_{max,\,i}\ln(1+b_i P_i^0(\pi)) \tag{S4}$$

Because, the reduced spreading pressures at the equilibrium state is taken to be equal for each component, hence:

$$z_1 = z_2 \tag{S5}$$

where subscripts 1 and 2 denotes CO_2 and N_2, respectively. On the other hand, by combining Eqs. (1), (4) and, (5), we have:

$$q_{max,\,CO_2}\ln\left(1+\frac{b_{CO_2}Py_{CO_2}}{x_{CO_2}}\right) - q_{max,\,N_2}\ln\left(1+\frac{b_{N_2}Py_{N_2}}{x_{N_2}}\right) = 0 \tag{S6}$$

where ($q_{max,\,CO_2}$, b_{CO_2}) and ($q_{max,\,N_2}$, b_{N_2}) are Langmuir fitting constants for pure CO_2 and N_2, respectively and the unknown parameter (x) could be calculated at known P and y. Consequently, following equation could be used for calculation of CO_2/N_2 selectivity (S_{CO_2/N_2}):

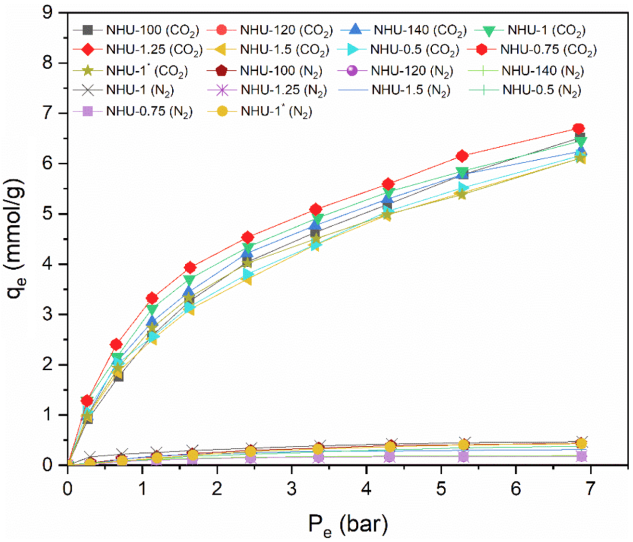


Fig. S1. CO_2 and N_2 adsorption capacity of all seven NH_2-UiO-66 at 25 °C.

$$S_{CO_2/N_2} = \frac{x_{CO_2}y_{N_2}}{x_{N_2}y_{CO_2}} \tag{S7}$$

Since in the current study, CO_2 and N_2 adsorption equilibrium data were fitted well with Langmuir isotherm model for all samples and in all experiments, the obtained constants were used to evaluate the performance of samples toward CO_2/N_2 separation.

2. CO_2 and N_2 Adsorption Capacity on Synthesized NH_2-UiO-66

Fig. S1 depicts CO_2 and N_2 adsorption capacity of all as-synthesized NH_2-UiO-66. It is clear that, NHU-120, NHU-1.25 and NHU-0.75 which are actually the same, showed the highest CO_2 and lowest N_2 adsorption capacity among all samples.

3. XRD Analysis

The XRD analysis for NHU-0.5, NHU-0.75 and NHU-1* is depicted in Fig. S2. As can be observed from Fig. S2, by raising the modulator to metal salt molar ratio, the intensity of the peaks at 2θ=7.4° and 2θ=8.5° became greater. In addition, the peaks at these points became narrower as well which means that a higher crystallinity of NH_2-UiO-66 is achieved with more amount of modulator [3]. This issue was also confirmed by FESEM micrographs where the crystals became more well-shaped by adding the M : S

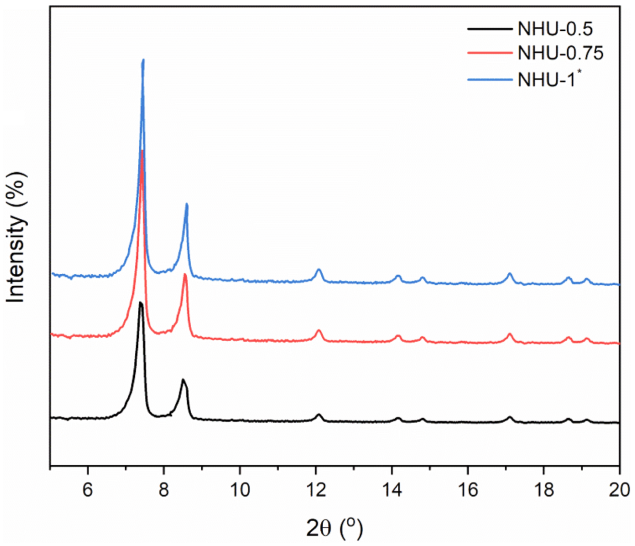


Fig. S2. Effect of different M : S molar ratio on XRD pattern of NH_2-UiO-66 crystal structure.

molar ratio.

4. FTIR Analysis

Fig. S3 represents the FTIR spectrum of UiO-66 and $Cu_3(BTC)_2$ and their aminated moieties. In Fig. S3(a), the band at 750 and 660 cm^{-1} might be associated with symmetric and asymmetric stretching O-Zr-O bonds, respectively [4]. The weak band at 1,500 cm^{-1} can be attributed to C=C aromatic absorption bond. At 1,570 cm^{-1} a sharp peak can be observed which is probably corresponded to the reaction of -COOH with Zr^{4+} ions [5]. In Fig. S3(a), for NH_2-UiO-66, an absorption band around 1,267 cm^{-1} is ascribed to C-N stretching free amine group. The symmetric and asymmetric NH_2 vibrating groups can be found at 3,410 and 3,505 cm^{-1} which belong to amine on the organic linker. Since there is an interaction between C=O groups of 2-amino terephthalic acid and the O-H groups of metal center, the intensity of the peak reduced which approves the presence of NH_2 groups [6]. FTIR spectrum of $Cu_3(BTC)_2$ was discussed in detail in our previous report [7]. From Fig. S3(b) it can be understood that there are some slight differences between the aminated $Cu_3(BTC)_2$ and its original one. The weak peak around

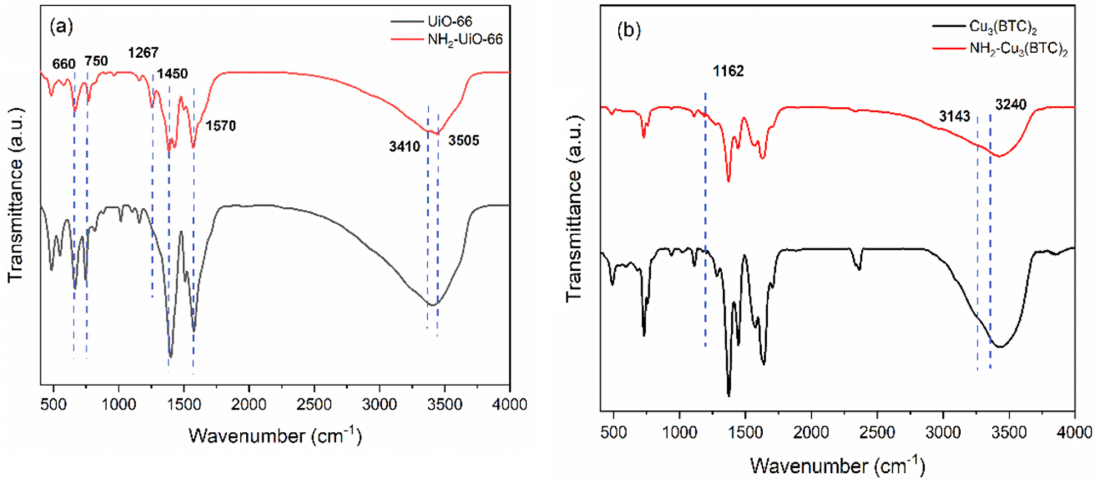


Fig. S3. FTIR spectrum of UiO-66, $Cu_3(BTC)_2$ and their aminated derivatives.

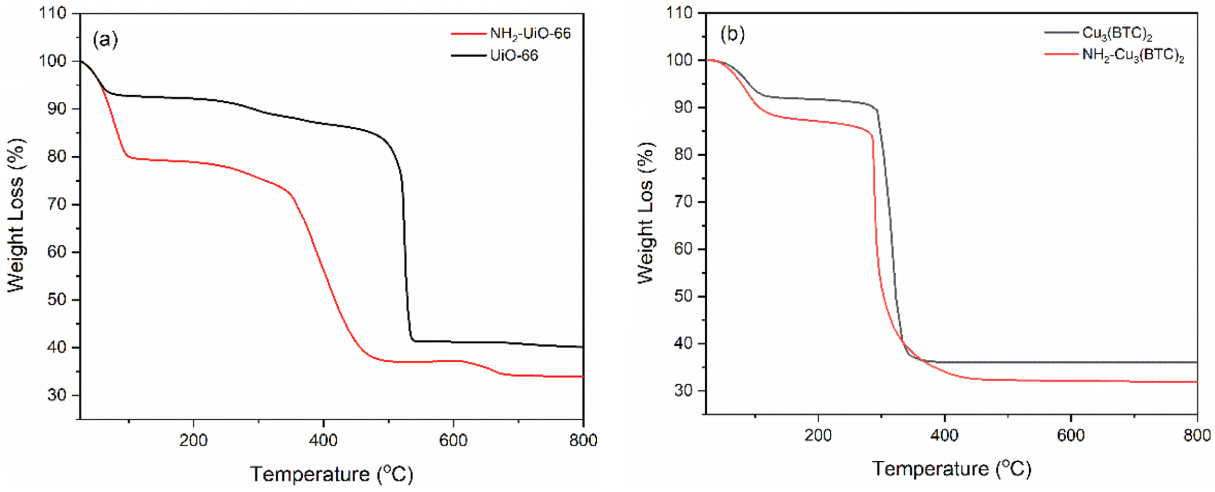


Fig. S4. TGA curves for UiO-66, $Cu_3(BTC)_2$ and their aminated derivatives.

1,162 cm^{-1} is ascribed to stretching C-N bond and peaks at 3,143 and 3,240 cm^{-1} are related to N-H bond that confirms the presence of amino group in NH_2-$Cu_3(BTC)_2$ [8].

5. TGA Analysis

Fig. S4 depicts the TGA plot for pristine and aminated UiO-66 and $Cu_3(BTC)_2$ which was carried out from 25 to 800 °C. In Fig. S3(a), it can be observed that there is a weight loss up to 100 °C which is related to the release of trapped water molecules. However, the moisture content in pristine sample was less (10 wt%) than the aminated one (20 wt%) which can be attributed to the presence of polar NH_2 groups. The second slight weight loss that occurred up to 350 and 500 °C for NH_2-UiO-66 and UiO-66, respectively are associates with the removal of solvent molecules (DMF) that did not exchange with ethanol. The drastic mass loss that happened around mentioned temperatures is assigned to the decomposition of ligands to the CO, CO_2 and ZrO_2 [9].

Fig. S4(b) shows thermal stability of NH_2-$Cu_3(BTC)_2$ and $Cu_3(BTC)_2$. Similar to Fig. S4(a), two major weight losses can be seen in thermogravimetric analysis of these samples. In the first section, the weight loss corresponds to the moisture removal that happens around 100 °C and after that there is an insignificant mass drop that is related to loss of ethanol from adsorbent pores and cages. The final drop that occurred for both samples around 300 °C is attributed to the decomposition of 2-aminoterephthalic and trimesic acid to copper oxide and metallic copper [10].

REFERENCES

1. P. Mishra, S. Mekala, F. Dreisbach, B. Mandal and S. Gumma, *Sep. Purif. Technol.*, **94**, 124 (2012).
2. R. Krishna, *Micropor. Mesopor. Mater.*, **156**, 217 (2012).
3. A. Huang, L. Wan and J. Caro, *Mater. Res. Bull.*, **98**, 308 (2018).
4. M. A. Rodrigues, J. de Souza Ribeiro, E. de Souza Costa, J. L. de Miranda and H. C. Ferraz, *Sep. Purif. Technol.*, **192**, 491 (2018).
5. H. R. Abid, J. Shang, H.-M. Ang and S. Wang, *Int. J. Smart Nano Mater.*, **4**, 72 (2013).
6. M. Vahidi, A. M. Rashidi and A. Tavasoli, *J. Iranian Chem. Soc.*, **14**, 2247 (2017).
7. K. Pirzadeh, A. A. Ghoreyshi, M. Rahimnejad and M. Mohammadi, *Korean J. Chem. Eng.*, **35**, 974 (2018).
8. B. Ge, Y. Xu, H. Zhao, H. Sun, Y. Guo and W. Wang, *Materials*, **11**, 1421 (2018).
9. M. Z. Ahmad, M. Navarro, M. Lhotka, B. Zornoza, C. Téllez, V. Fila and J. Coronas, *Sep. Purif. Technol.*, **192**, 465 (2018).
10. Y. Wang, H. Ge, Y. Wu, G. Ye, H. Chen and X. Hu, *Talanta*, **129**, 100 (2014).